ISSN 1063-7834, Physics of the Solid State, 2018, Vol. 60, No. 10, pp. 2072–2077. © Pleiades Publishing, Ltd., 2018.
Original Russian Text © L.E. Bykova, V.S. Zhigalov, V.G. Myagkov, M.N. Volochaev, A.A. Matsynin, G.N. Bondarenko, G.S. Patrin, 2018, published in Fizika Tverdogo Tela, 2018, Vol. 60, No. 10, pp. 2028–2032.

LOW-DIMENSIONAL SYSTEMS

$Co–In_2O_3$ Nanocomposite Films: Synthesis and Structural and Magnetic Properties

L. E. Bykova[a, *], V. S. Zhigalov[a], V. G. Myagkov[a], M. N. Volochaev[a, b], A. A. Matsynin[a], G. N. Bondarenko[c], and G. S. Patrin[a, d]

[a] *Kirensky Institute of Physics, Krasnoyarsk Scientific Center, Siberian Branch, Russian Academy of Sciences, Krasnoyarsk, 630090 Russia*

[b] *Siberian University of Science and Technology, Krasnoyarsk, 630014 Russia*

[c] *Institute of Chemistry and Chemical Technology, Krasnoyarsk Scientific Center, Siberian Branch, Russian Academy of Sciences, Krasnoyarsk, 630090 Russia*

[d] *Siberian Federal University, Krasnoyarsk, 660041 Russia*

**e-mail: lebyk@iph.krasn.ru*

Received April 2, 2018

Abstract—The structural and magnetic properties of granular $Co–In_2O_3$ nanocomposite films formed by vacuum annealing of In/Co_3O_4 film bilayers at a temperature of 550°C have been investigated. The synthesized $Co–In_2O_3$ films contain ferromagnetic cobalt nanoclusters with an average size of 60 nm and a magnetization of ~340 emu/cm^3 surrounded by the In_2O_3 layer and exhibit the thermally activated conductivity.

DOI: 10.1134/S1063783418100049

1. INTRODUCTION

Granular nanocomposites consisting of ferromagnetic nanoparticles embedded in semiconductor (In_2O_3, TiO_2, ZnO, and SnO_2) or dielectric (SiO_2, Al_2O_3, MgO, and ZrO_2) matrices have been intensively studied as objects interesting both for fundamental research and application [1–3]. The magnetic and physicochemical properties of these nanocomposites strongly depend on a fabrication technique used, particle size and concentration, and a type of chemical bond between nanoparticles and a matrix. Granular nanomaterials are often prepared by wet chemical methods, including a sol-gel method, spray pyrolysis, a microemulsion method [4–6], magnetron sputtering, pulsed laser deposition, ion implantation [7–9], and joint deposition [10]. However, the search for new ways of creating hybrid film nanocomposites is of great importance. In our previous works [11–17], we discussed a new approach to the synthesis of ferromagnetic nanocomposite film materials based on the initiation of thermite reactions between the films of Fe_2O_3 and Co_3O_4 3*d* metal oxides and In, Zr, Zn, and Al metals, the oxides of which represent wide-gap semiconductors or dielectrics. Granular films containing iron nanoparticles in the In_2O_3, ZrO_2, and Al_2O_3 oxide matrices [11–13], cobalt in the ZrO and Al_2O_3 matrices [14, 15], FePt in the Al_2O_3 matrix [16], and magnetite Fe_3O_4 in the ZnO matrix [17] were obtained.

$Co–In_2O_3$ nanocomposites and cobalt-doped In_2O_3 attract attention due to their possible use in optoelectronic and spintronic [18–21] devices and gas sensors [22–25].

This paper presents the results of investigations of the structural and magnetic properties of the granular $Co–In_2O_3$ nanocomposite films obtained by initiating a thermite reaction in the In/Co_3O_4 film system by vacuum annealing at a temperature of 550°C.

2. EXPERIMENTAL

Synthesis of the granular $Co–In_2O_3$ film nanocomposites followed the thermite reaction

$$3Co_3O_4 + 8In \rightarrow 4In_2O_3 + 9Co \quad (1)$$

in the In/Co_3O_4 film bilayer and consisted of the two stages:

1. Fabrication of the In/Co_3O_4 film bilayers, including

(i) thermal deposition of Co films with a thickness of ~50 nm in vacuum at a residual pressure of 10^{-6} Torr onto 0.18-mm-thick glass substrates preliminary degassed for an hour at a temperature of 350°C,

(ii) formation of Co_3O_4 films by air oxidation of Co layers at 450°C for 30 min, and

(iii) thermal deposition of the In layer with a thickness of ~100 nm in vacuum at a residual pressure of 10^{-6} Torr onto the Co_3O_4 film surface. To prevent an

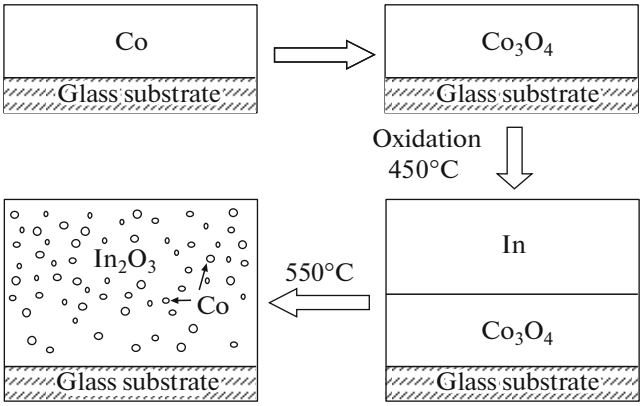

Fig. 1. Block diagram of the thermite synthesis of the Co–In_2O_3 nanocomposite films.

uncontrolled reaction between the In and Co_3O_4 layers, In was deposited at room temperature.

2. Annealing of the obtained In/Co_3O_4 samples in vacuum at a residual pressure of 10^{-6} Torr in the temperature range of 50–550°C with a step of 50°C and exposure at each temperature for 30 min.

The In and Co layer thicknesses were determined by X-ray fluorescence analysis. Magnetization was measured on a rotating coil magnetometer using the technique proposed in [26]. Phase composition was studied by X-ray diffraction on a DRON-4-07 diffractometer in CuK_α radiation with a wavelength of 0.15418 nm. Structural investigations of the initial and synthesized films were carried out by transmission electron microscopy on a Hitachi HT7700 microscope equipped with a Bruker X-Flash 6T/60 energy dispersive spectrometer at an accelerating voltage of 100 kV. For this purpose, In/Co_3O_4/NaCl(001) films with a Co_3O_4 layer thicknesses of 20 nm and an In layer thickness of 40 nm were prepared. The films were then separated from the NaCl substrate in distilled water, deposited on a transmission electron microscope support grid, and annealed in vacuum at a residual pressure of 10^{-6} Torr at 550°C.

Cross sections were prepared using a Hitachi FB2100 focused ion beam (FIB) system according to the procedure described in [27]; to prevent sample destruction during cutting, the samples were preliminary coated with a protective amorphous germanium film.

All the measurements were performed at room temperature.

The temperature dependence of the resistance of the In/Co_3O_4 film was measured by a four-probe method using pressed contacts in vacuum at a residual pressure of 10^{-6} Torr and a heating rate of ~5°C/min.

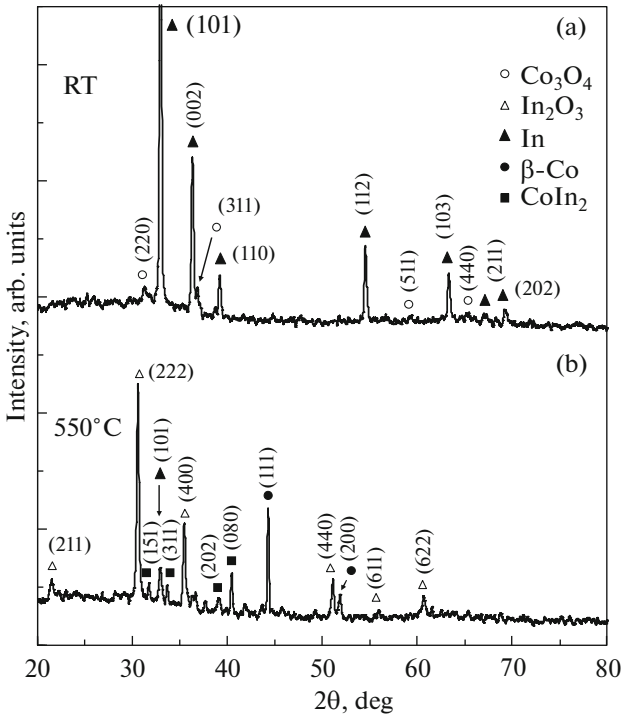

Fig. 2. X-ray diffraction patterns of (a) the initial In/Co_3O_4 film and (b) the film annealed at 550°C.

3. RESULTS AND DISCUSSION

The block diagram of the thermite synthesis of Co–In_2O_3 nanocomposite films is shown in Fig. 1. According to the X-ray spectrum, which only contained In and polycrystalline Co_3O_4 reflections (Fig. 2a), the initial In/Co_3O_4 samples were film bilayers. The diffraction patterns obtained on the films annealed at 300 and 400°C showed only a decrease in the indium peaks and occurrence of the In_2O_3 peaks. Cobalt reflections were not observed because of the minor amount of cobalt and its high dispersity. After annealing at 500°C, the diffraction pattern drastically changed; the β-Co and In_2O_3 peaks occurred and the low peaks corresponding to unreacted indium and $CoIn_2$ were observed, which did not change upon annealing at 550°C (Fig. 2b).

The electron diffraction pattern of the initial samples (Fig. 3) also confirmed the formation of the In/Co_3O_4 film bilayer, since it only contained the In and polycrystalline Co_3O_4 reflections (Table 1). The electron diffraction pattern of the samples annealed at 550°C (Fig. 4) contained the β-Co, In_2O_3, CoO, and $CoIn_2$ reflections (Table 2).

Figure 5a shows the annealing temperature dependence of the relative saturation magnetization M_S/M_0 for the In/Co_3O_4 film sample, where M_0 = 1400 emu/cm^3 is the saturation magnetization of the initial Co film, which coincides with the saturation

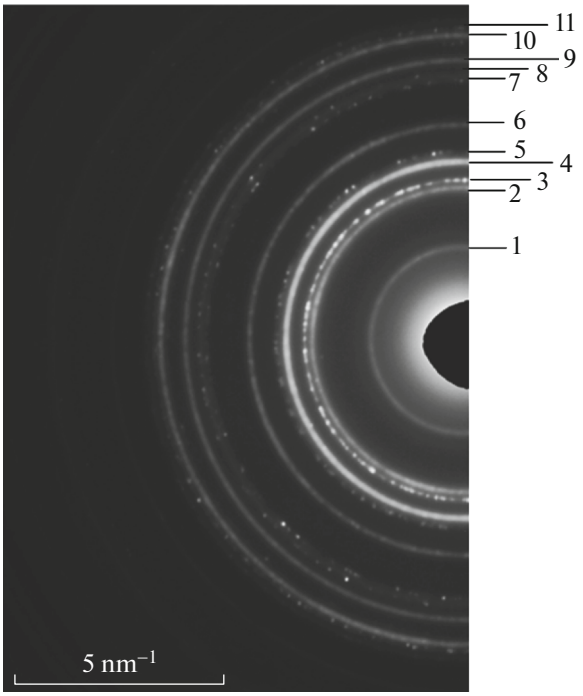

Fig. 3. Electron diffraction pattern of the initial In/Co_3O_4 film.

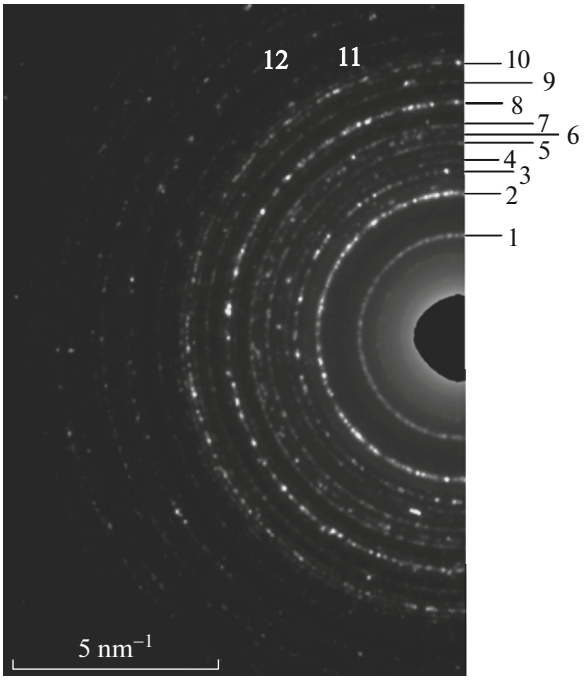

Fig. 4. Electron diffraction pattern of the In/Co_3O_4 film annealed at 550°C.

magnetization of the bulk samples. The In/Co_3O_4 samples annealed at temperatures below 150°C were nonmagnetic because the In and Co_3O_4 layers do not react with each other. Annealing at 200°C led to the occurrence of the saturation magnetization M_S indicative of the onset of solid-phase reaction (1) and the formation of Co nanoparticles. After annealing at 500°C, the magnetization M_S took its maximum value and did not change upon annealing at 550°C, which corresponded to the end of reaction (1). The ratio M_S/M_0 indicates the degree of cobalt recovery. It can be seen in Fig. 5a that approximately 70% of Co recovered after annealing at 550°C and the rest Co passed to the nonmagnetic CoO and $CoIn_2$ phases, according to the X-ray and electron microscopy data (Fig. 2b and Table 2). The inset in Fig. 5a shows a room-temperature hysteresis loop for the synthesized Co–In_2O_3 nanocomposite film, according to which the film magnetization is ~340 emu/cm^3 and the coercivity is Hc ~ 80 Oe. These values were stable and did not change with time.

Table 1. Identification of the diffraction reflections of the initial In/Co_3O_4 film

Rings	Co_3O_4	In
1	111	
2	220	
3		101
4	222	
5		110
6	400	
7		112
8		200
9	511	
10	440	
11		202

Table 2. Identification of the diffraction reflections of the In/Co_3O_4 film annealed at 550°C

Rings	In_2O_3	β-Co	CoO	$CoIn_2$
1	211			
2	222			
3	400			
4	411			400
5			200	242
6		111		
7	431			
8	440	200		
9	611			
10	622		220	462
11	721			
12	741	220		

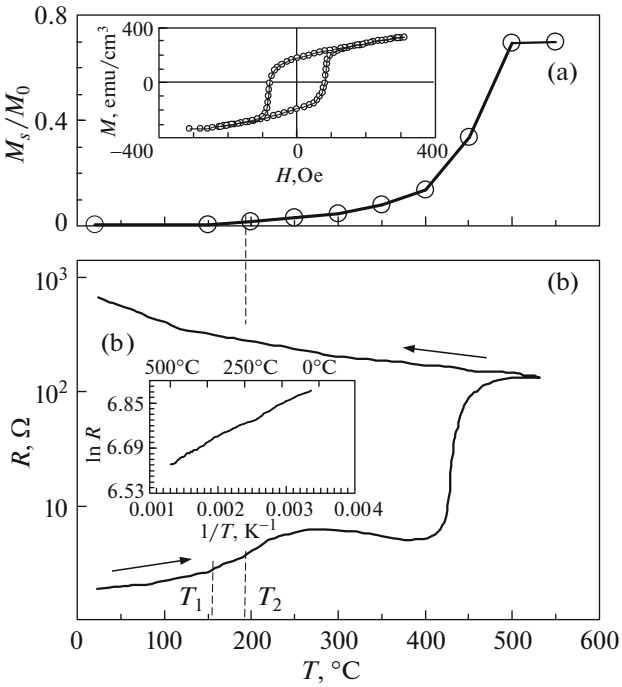

Fig. 5. (a) Magnetization of the In/Co_3O_4 film as a function of annealing temperature T. Inset: hysteresis loop of the synthesized Co–In_2O_3 nanocomposite film. (b) Electrical resistance of the In/Co_3O_4 film as a function of annealing temperature T. Inset: ln$R(T^{-1})$ plot upon cooling the film from 500°C to room temperature.

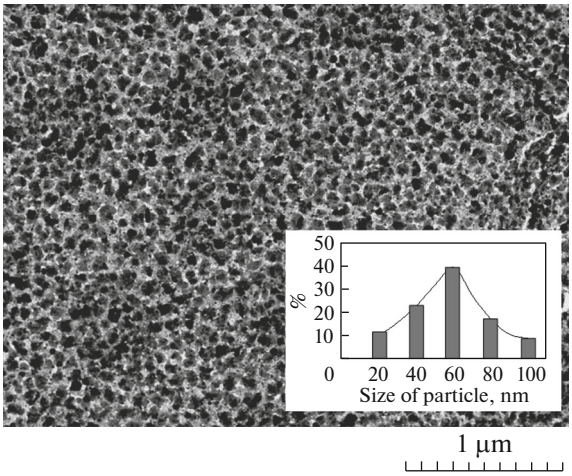

Fig. 6. Electron microscopy image of the Co–In_2O_3 nanocomposite film and histogram of size distribution of Co nanoparticles.

The measured electrical resistance R of the In/Co_3O_4 samples as a function of the annealing temperature T (Fig. 5b) is consistent with the results of temperature measurements of the saturation magnetization M_S for these samples (Fig. 5a). The resistance of the In/Co_3O_4 film is initially metallic, which is determined by the upper indium layer. A slight increase in the resistance is observed near the indium melting point T_1 = 156°C. Above T_2 = 190°C, the resistance increases, which is caused by the start of reaction (1). A slight decrease in the resistance above 250°C is probably due to the formation of cobalt nanograins. As the temperature increases above 400°C, the resistance sharply grows, which is related to the reaction relaxation processes, including the increase in the size of Co grains and improvement of their crystal quality in the insulating In_2O_3 matrix. According to the X-ray and electron microscopy data, the reaction completely ends at a temperature of 550°C. Cooling the samples to room temperature led to an increase in the resistance, which is typical of semiconductors.

The inset in Fig. 5b shows the ln$R(T^{-1})$ plot for the synthesized Co–In_2O_3 nanocomposite upon cooling to 25°C. It was found that the logarithm of the R plot below 500°C is linearly proportional to the reciprocal temperature T^{-1} (the conductivity activation energy is $E_a \sim 0.02$ eV). This result shows that the obtained Co–In_2O_3 nanocomposite is characterized by the thermally activated conductivity, which is characteristic of most granular metallic films at these temperatures [28].

It follows from the temperature dependence of the electrical resistance $R(T)$ (Fig. 5b) and dependence of the magnetization variation on the annealing temperature T (Fig. 5a) for the In/Co_3O_4 bilayers that the temperature of initiation of reaction (1) is $T_{in} = T_2 \approx$ 190°C.

The average cobalt grain size d in the obtained film was estimated from the β-Co(111) reflection broadening in the diffraction pattern presented in Fig. 2b using the Scherrer formula [29]. The obtained value of $d \approx$ 60 nm agrees well with the electron microscopy data (Fig. 6). The electron microscopy image shows that Co nanoparticles are uniformly distributed in the reaction product. The average atomic number of the In_2O_3 phase is smaller than the Co atomic number; therefore, the In_2O_3 region appears brighter in the image (Fig. 6) as compared with the Co region. The dark regions correspond to Co grains and the bright regions, to the In_2O_3 matrix. The histogram in Fig. 6 shows that the average diameter of Co nanoparticles is ~60 nm. However, Co nanoparticles smaller than 20 nm were not included in the histogram, since they are not resolved in the electron microscopy image. The cross section and elemental composition of the Co–In_2O_3 film show that a cobalt particle is surrounded by indium and oxygen (Fig. 7). This confirms the formation of ferromagnetic cobalt nanoclusters surrounded by the In_2O_3 layer in the reaction products.

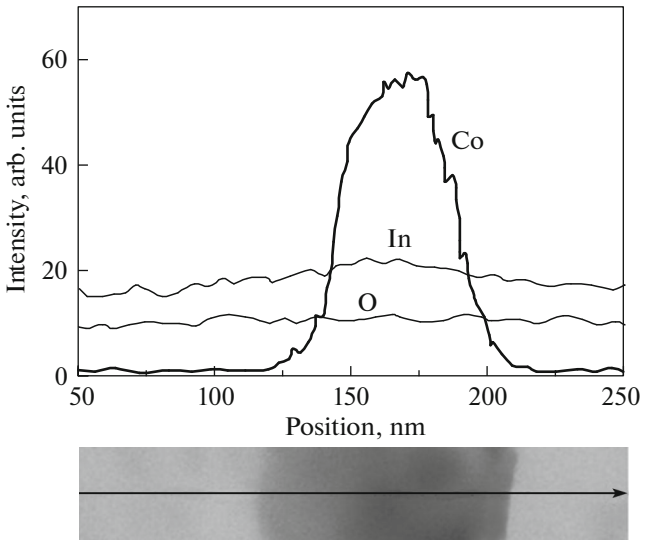

Fig. 7. Cross section and elemental composition of the $Co–In_2O_3$ nanocomposite film.

All the synthesized $Co–In_2O_3$ samples had hysteresis loops (inset in Fig. 5a); this means that the Co nanoparticle size exceeds a superparamagnetic size of ~20 nm typical of Co nanoparticles [30]. The absence of saturation in the fields stronger than the coercivity suggests that the synthesized $Co–In_2O_3$ samples contain a certain amount of superparamagnetic Co nanoparticles ($d < 20$ nm). These particles and disordered spins at the Co/In_2O_3 interface contribute to the strong-field portion of the hysteresis loop of the $Co–In_2O_3$ film. The relatively large ratio $M_r/M_S \sim 0.6$ between the remanent magnetization M_r and saturation magnetization M_S (Fig. 5) shows that Co nanoparticles consist of randomly oriented grains with the cubic magnetocrystalline anisotropy [31].

The electron microscopy measurements were performed on the equipment of the Center of Collective Use of the Krasnoyarsk Scientific Center, Russian Academy of Sciences, Siberian Branch.

4. CONCLUSIONS

Thus, the main results of our investigations are as follows. The ferromagnetic $Co–In_2O_3$ composite films were obtained using solid-state reaction (1) in the In/Co_3O_4 layered structure. The reaction initiation temperature was found to be ~190°C. A complex of the structural and magnetic investigations unambiguously revealed the formation of ferromagnetic cobalt nanoclusters with an average size of 60 nm, a magnetization of 340 emu/cm^3, and a room-temperature coercivity of H_c ~80 Oe surrounded by the In_2O_3 layer in the reaction products. Thus, the termite method is promising for synthesizing ferromagnetic nanocomposite thin films consisting of ferromagnetic clusters embedded in oxide matrices and characterized by the high magnetization and chemical stability.

ACKNOWLEDGMENTS

This study was supported by the Russian Foundation for Basic Research, project no. 16-03-00069 and, in part, by the Grant Council of the President of the Russian Federation, project no. SP-1373.2016.3 and the Russian Foundation for Basic Research and the Government of the Krasnoyarsk Territory, project no. 18-42-243009r_mol_a.

REFERENCES

1. X. Batlle and A. Labarta, J. Phys. D **35**, R15 (2002).
2. A. Pucci, G. Clavel, M.-G. Willinger, D. Zitoun, and N. Pinna, J. Phys. Chem. C **113**, 12048 (2009).
3. T. Wen and K. M. Krishnan, J. Phys. D **44**, 393001 (2011).
4. J. T. Jiang, X. J. Wei, C. Y. Xu, Z. X. Zhou, and L. Zhen, J. Magn. Magn. Mater. **334**, 111 (2013).
5. M. Baikousi, O. Kostoula, I. Panagiotopoulos, T. Bakas, A. P. Douvalis, I. Koutselas, A. B. Bourlinos, and M. A. Karakassides, Thin Solid Films **520**, 159 (2011).
6. J. Okabayashi, S. Kono, Y. Yamada, and K. Nomura, AIP Adv. **1**, 042138 (2011).
7. A. Butera, J. N. Zhou, and J. A. Barnard, J. Appl. Phys. **87**, 5627 (2000).
8. C. Chen, O. Kitakami, S. Okamoto, and Y. Shimada, J. Appl. Phys. **86**, 2161 (1999).
9. J. Gómez, A. Butera, and J. A. Barnard, Phys. Rev. B **70**, 054428 (2004).
10. O. Santini, D. H. Mosca, W. H. Schreiner, R. Marangoni, J. L. Guimaraes, F. Wypych, and A. J. A. de Oliveira, J. Phys. D **36**, 428 (2003).
11. V. G. Myagkov, I. A. Tambasov, O. A. Bayukov, V. S. Zhigalov, L. E. Bykova, Yu. L. Mikhlin, M. N. Volochaev, and G. N. Bondarenko, J. Alloys Compd. **612**, 189 (2014).
12. I. A. Tambasov, K. O. Gornakov, V. G. Myagkov, L. E. Bykova, V. S. Zhigalov, A. A. Matsynin, and E. V. Yozhikova, Phys. B (Amsterdam, Neth.) **478**, 135 (2015).
13. V. G. Myagkov, L. E. Bykova, O. A. Bayukov, V. S. Zhigalov, I. A. Tambasov, S. M. Zharkov, A. A. Matsynin, and G. N. Bondarenko, J. Alloys Compd. **636**, 223 (2015).
14. V. G. Myagkov, V. S. Zhigalov, L. E. Bykova, S. M. Zharkov, A. A. Matsynin, M. N. Volochaev, I. A. Tambasov, and G. N. Bondarenko, J. Alloys Compd. **665**, 197 (2016).
15. V. G. Myagkov, L. E. Bykova, V. S. Zhigalov, A. A. Matsynin, M. N. Volochaev, I. A. Tambasov, Yu. L. Mikhlin, and G. N. Bondarenko, J. Alloys Compd. **724**, 820 (2017).
16. V. S. Zhigalov, V. G. Myagkov, L. E. Bykova, G. N. Bondarenko, A. A. Matsynin, and M. N. Volochaev, Phys. Solid State **59**, 392 (2017).

17. L. E. Bykova, V. G. Myagkov, I. A. Tambasov, O. A. Bayukov, V. S. Zhigalov, K. P. Polyakova, G. N. Bondarenko, I. V. Nemtsev, V. V. Polyakov, G. S. Patrin, and D. A. Velikanov, Phys. Solid State **57**, 386 (2015).
18. Z.-K. Tang, L.-M. Tang, D. Wang, L.-L. Wang, and K.-Q. Chen, Eur. Phys. Lett. **97**, 57006 (2012).
19. X. Meng, L. Tang, and J. Li, J. Phys. Chem. C **114**, 17569 (2011).
20. R. Mukherji, V. Mathur, A. Samariya, and M. Mukherji, J. Adv. Nanomater. **2**, 105 (2017).
21. N. H. Hong, J. Sakai, N. T. Huong, and V. Brizé, J. Magn. Magn. Mater. **302**, 228 (2006).
22. M. Z. Naik and A. V. Salker, Mater. Res. Innovations **21**, 237 (2017).
23. Z. Li and Y. Dzenis, Talanta **85**, 82 (2011).
24. Z. Wang, C. Hou, Q. De, F. Gu, and D. Han, ACS Sens. **3**, 468 (2018).
25. L. A. Obvintseva, Ros. Khim. Zh. **52**, 113 (2008).
26. S. Chikazumi, J. Appl. Phys. **32**, S81 (1961).
27. M. N. Volochaev and Yu. Yu. Loginov, Vestn. SibGAU **17**, 792 (2016).
28. C. A. Neugebauer and M. B. Webb, J. Appl. Phys. **33**, 7482 (1962).
29. P. Scherrer and N. G. Wissen, Gottingen. Math.- Phys. **K1**, 98 (1918).
30. A. I. Gusev and A. A. Rempel, *Nanocrystalline Materials* (Cambridge Int. Sci., Cambridge, 2003).
31. *Nanoparticles and Nanostructured Films: Preparation, Characterization and Applications*, Ed. by J. H. Fendle (Wiley-VCH, Weinheim, 2008).

Translated by E. Bondareva